ACS OMEGA

Open Access

http://pubs.acs.org/journal/acsodf

Article

Reduction in Marine Primary Productivity in the Early Cambrian Nanhua Basin, South China

Chengsheng Jin,* Zihu Zhang, Meng Cheng, Guochang Wang, Huajin Chang, Zhengqi Cao, and Tao Zhang*

Cite This: *ACS Omega* 2024, 9, 19892−19903

Read Online

ACCESS | Metrics & More | Article Recommendations | Supporting Information

ABSTRACT: The Cambrian explosion is represented by a rapid diversification of early animals in which the role of marine primary productivity remains obscure. In this study, we analyzed multiple geochemical data, including TOC, major, and trace elements, in the basinal Yuanjia section, South China. Covariations among TOC, P/Al, Cu_{EF}, and Ni_{EF} suggest that they could be taken as effective marine productivity proxies in the early Cambrian Nanhua Basin. The similarities of Cd_{EF} and Cd/Mo in the Nanhua Basin and modern upwelling settings suggest that they might be effective to track upwelling, where Cd and Mo were mainly controlled by plankton biomass and redox conditions, respectively. Our results indicate that Co_{EF} and Co × Mn were invalid in evaluating upwelling because of the significant effects of water-column redox conditions on Co enrichments in the Nanhua Basin. The decreased TOC, P/Al, Cu_{EF}, and Ni_{EF} reflect a long-term decline in marine productivity from late age 2 to age 3. In comparison with the published results in the outer shelf (Jinsha, TZS drill core, YJK drill core, and GDM-1 well) and slope areas (TX-1 well), the fall in marine productivity might be common in the early Cambrian Nanhua Basin. Our results exhibit that the reduced marine productivity was accompanied by weakened upwelling, quiet hydrothermal activities, and enhanced local terrestrial fluxes, indicating that variations in marine productivity might be mainly driven by the development of upwelling in the early Cambrian Nanhua Basin. Comparison of marine productivity with fossil records suggests that food availability was sufficient to sustain the Cambrian explosion in the Nanhua Basin. We infer that marine productivity might indirectly stimulate early animal evolution through its significant impact on water-column oxygen levels in the early Cambrian Nanhua Basin.

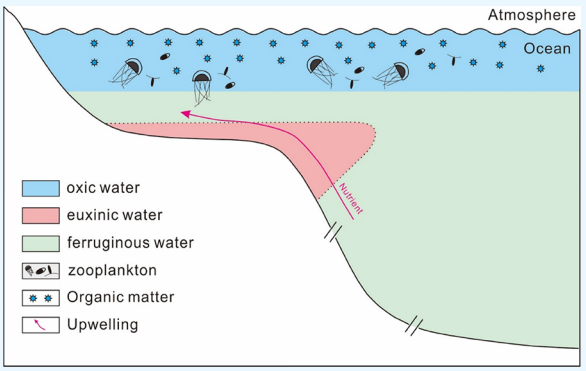

1. INTRODUCTION

The early Cambrian witnessed the occurrences of almost all metazoan phyla for the first time in Earth's history, which is widely known as the Cambrian explosion.[1,2] It is well accepted that large, active animals have higher physiological requirement for oxygen relative to small, inactive animals.[3] Therefore, the enhanced oxygenation of the oceanic systems has been widely invoked for metazoan evolution during the early Cambrian.[3] On the other hand, a shift in primary producers from small, cyanobacteria-dominated phytoplankton to large, eukaryotic-dominated phytoplankton occurred in the early Cambrian Ocean, which might significantly enhance the complexity of food webs.[4] Accordingly, marine productivity has been frequently taken as another important trigger for the Cambrian explosion.[5] Moreover, marine redox conditions are closely connected with marine productivity on local and global scales.[6,7] For example, local marine redox conditions are strongly affected by the availability of organic matter that might be driven by local marine productivity.[6] Meanwhile, marine redox conditions globally might be controlled by atmospheric oxygen levels, which might possibly result from the burial of organic matter in association with marine productivity.[7] For these reasons, the possible oxygen and productivity triggers can be strongly linked during the Cambrian explosion.

There are a large number of research studies on oceanic oxygen levels during the early Cambrian.[8−10] In contrast, a few studies focused on marine productivity in the early Cambrian, yielding some controversial results. For example, compilations of total organic carbon (TOC) and $\delta^{15}N_{TN}$ in the sediment suggest a rise in marine productivity, resulting in the Cambrian explosion.[5,11] However, $\delta^{15}N_{TN}$ data indicate that both Chengjiang and Qingjiang biotas thrive in low productivity even oligotrophic environments during the peak Cambrian

Received: November 17, 2023
Revised: April 9, 2024
Accepted: April 11, 2024
Published: April 25, 2024

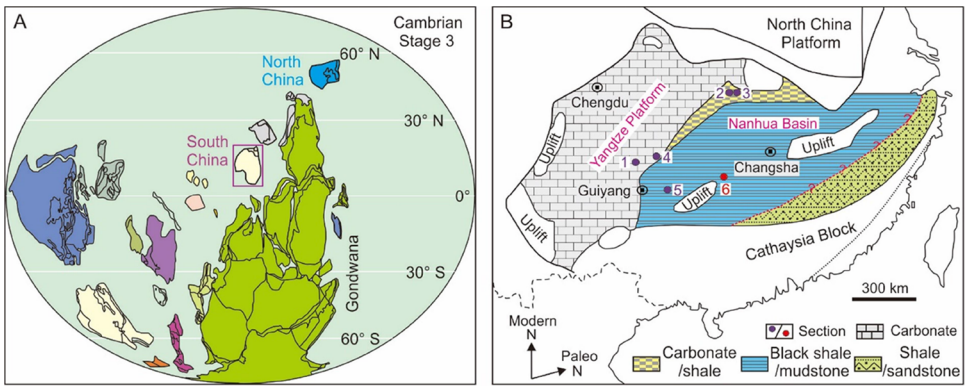

Figure 1. Locality and paleogeography of South China during the early Cambrian. (A) Global paleogeography.[23] Copyright 2015 Elsevier Ltd. (B) Paleogeography of South China.[24] Copyright 2007 Elsevier Ltd. Sections: 1—Jinsha, 2—TZS drill core, 3—JYK drill core, 4—GDM-1 well, 5—TX-1 well, and 6—Yuanjia.

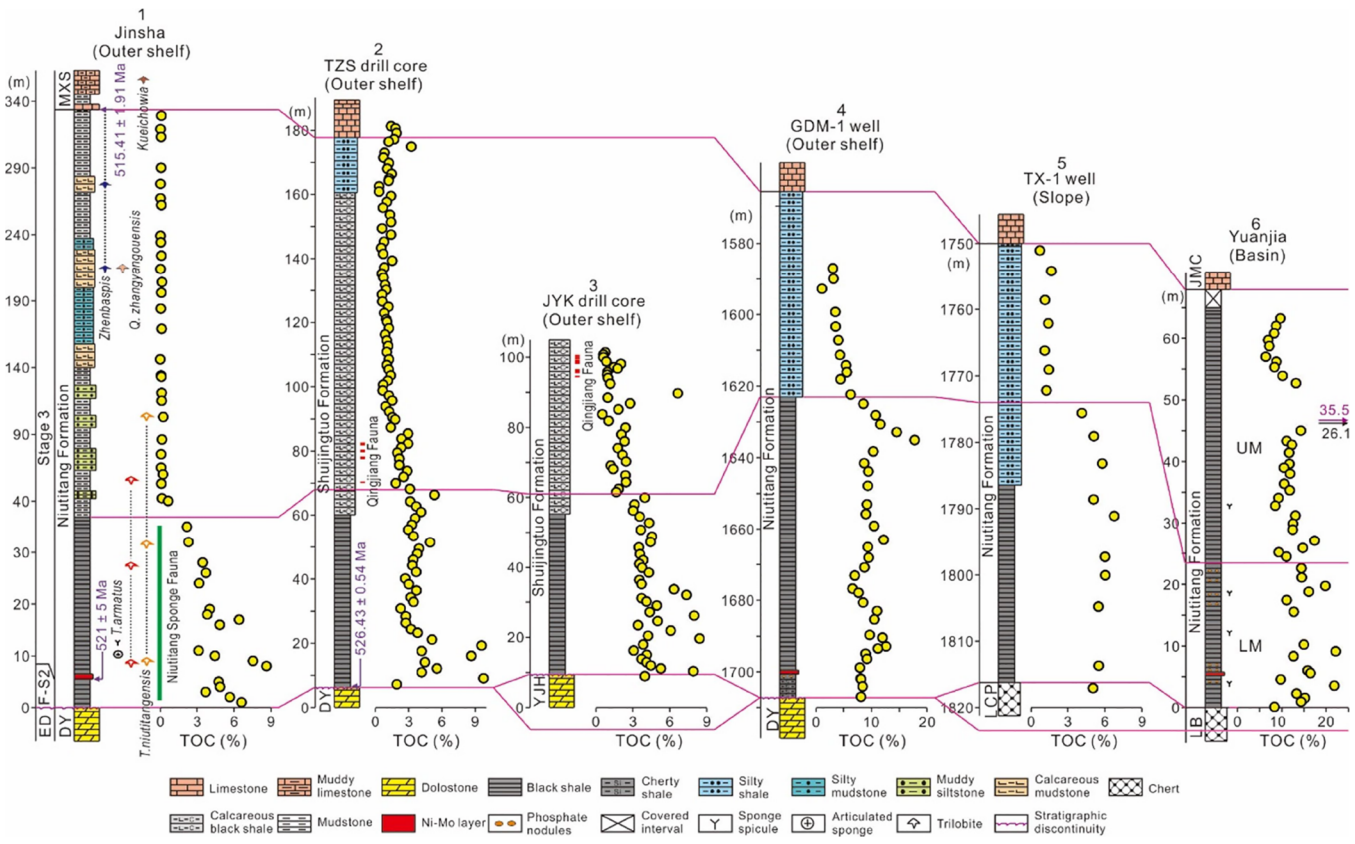

Figure 2. Stratigraphic framework in the early Cambrian Nanhua Basin. Sections: 1—Jinsha,[9] 2—TZS drill core,[12] 3—JYK drill core,[12] 4—GDM-1 well,[16] 5—TX-1 well,[16] 6—Yuanjia (this study). The U−Pb age of 526.43 ± 0.54 Ma is from Yang et al.[33] The Re−Os age of 521 ± 5 Ma for the Ni−Mo layer is from Xu et al.[35] The age of 515.41 ± 1.91 Ma based on cyclostratigraphic analysis is from Zhang et al.[39] Abbreviations: ED—Ediacaran; F-S2—Fortunian-Stage 2; DY—Dengying Formation; YJH—Yanjiahe Formation; MXS—Mingxinsi Formation; L—Liuchapo Formation; LB—Laobao Formation; JMC—Jiumenchong Formation; LM—Lower member; and UM—Upper member.

explosion, making the influence of marine productivity on the Cambrian explosion unclear.[12]

The early Cambrian marine productivity has been considered to be controlled by many factors, particularly the terrestrial input, upwelling, and hydrothermal activity, which can separately supply nutrients from the continent, deep ocean, and hydrothermal fluids to the oceanic euphotic zone, respectively. The terrestrial fluxes can be evaluated by continental basement rocks, precipitation of carbonate sediments, proportion of glauconite-rich siliciclastic rock units, $^{87}Sr/^{86}Sr$, and εNd.[13] The developments of upwelling can be constrained by the proxies of Co × Mn and Cd/Mo in organic-rich sediments.[14,15] The signals of hydrothermal fluids can be documented by multiple geochemical proxies, such as Eu/Eu*,[16−18] Fe/Ti,[19,20] Al/(Al+Mn+Fe),[19−21] Hg contents, and Hg isotopes.[17]

In this study, we report geochemical data of paleoproductivity (Cu_{EF}, Ni_{EF}, and P/Al), hydrothermal activities (Fe/Ti, Al/(Al+Mn+Fe), and Eu/Eu*), and local terrestrial fluxes (Al and Th) from the basinal Yuanjia section in South China. In combination with previously published data from the same section and other contemporary sections in the Nanhua Basin, this study provides

https://doi.org/10.1021/acsomega.3c09161
ACS Omega 2024, 9, 19892−19903

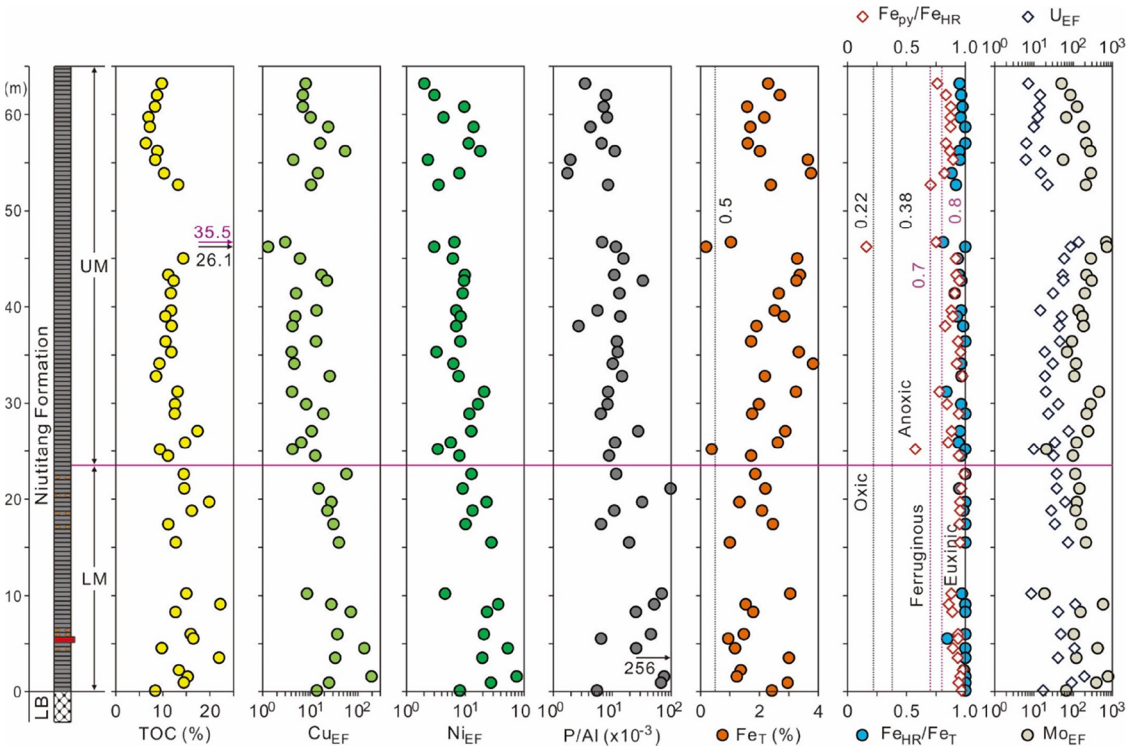

Figure 3. Geochemical results for productivity and redox conditions are given in the Yuanjia section. Fe_{HR}/Fe_T < 0.22 and >0.38 point to oxic and anoxic conditions, respectively.[14] When anoxia is indicated, Fe_{py}/Fe_{HR} < 0.7−0.8 and >0.7−0.8 reflect ferruginous and euxinic states, respectively.[14] The redox interpretations of Fe speciation proxies are effective for sedimentary rocks with Fe_T >0.5%. TOC, Fe speciation, Mo_{EF}, and U_{EF} are from Chen et al.[14] and Cheng et al.[40]

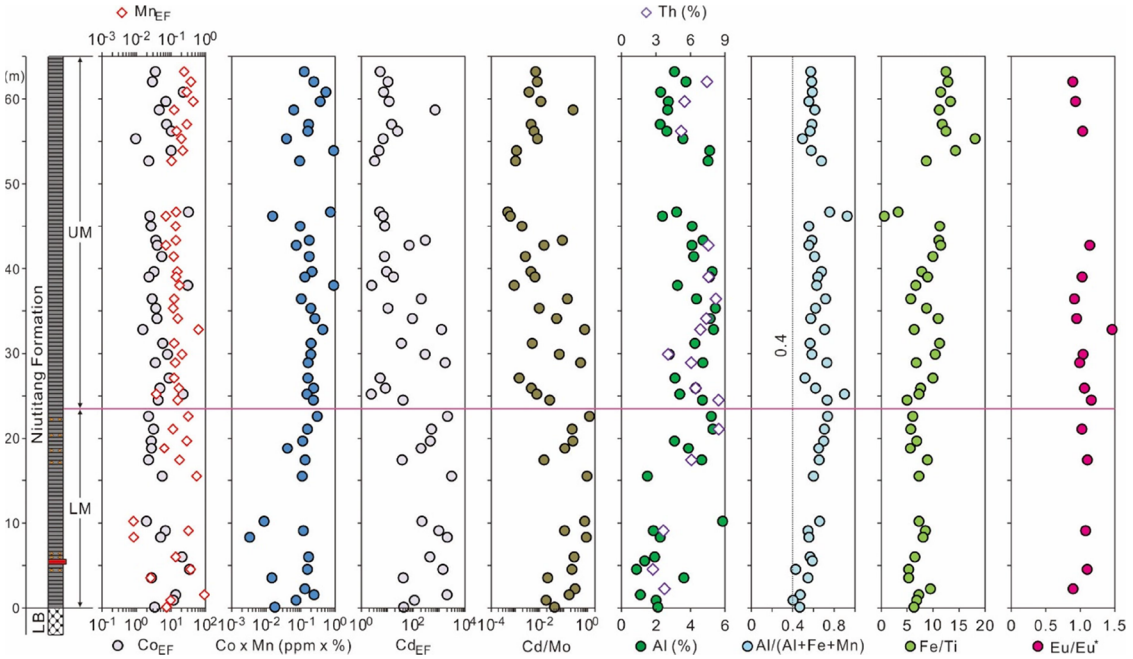

Figure 4. Geochemical results for upwelling, terrigenous fluxes, and hydrothermal activity are given in the Yuanjia section. The distinguishment between hydrothermal activities (Al/(Al+Fe+Mn) < 0.4) and terrigenous fluxes (Al/(Al+Fe+Mn) > 0.4) are according to Sylvestre et al.[61]

new insights into the fluctuations of marine productivity and their causes during the early Cambrian.

2. GEOLOGICAL SETTING

2.1. Paleogeography and Study Sections. The South China craton was located in the northwest of the Gondwana supercontinent during the early Cambrian (Figure 1A).[22,23] It included the Yangtze Block in the northwest and the Cathaysia Block in the southeast (Figure 1B).[24] The early Cambrian Yangtze Block was composed of shelf, transitional, and slope−basinal settings from the northwest to the southeast (Figure 1B). The shelf facies comprised dolomite, limestone, and phosphor-

https://doi.org/10.1021/acsomega.3c09161
ACS Omega 2024, 9, 19892−19903

ite from Cambrian Fortunian Age to early Age 2, whereas the coeval slope−basinal facies were mainly composed of chert.[9] The transitional zone consisted of dolomite and limestone interbedded with shale during the same period.[25] During late age 2, the whole Yangtze Block was almost covered by black shale due to a marine transgression.[9]

The Yuanjia section (27°29′25″N, 110°14′46″E) is located in Huaihua City, Hunan Province, which is deposited in a basinal setting. In ascending order, the lower Cambrian strata at Yuanjia comprise the upper Liuchapo, Niutitang, and Jiumenchong formations (Figure 2). All samples are collected from the Niutitang Formation because the coeval strata record many geological events, such as the radiations of early animals, enhanced ocean oxygenation, and high marine productivity. The Niutitang Formation comprises black shale, a Ni−Mo layer, and two layers of phosphate nodules, where a few sponge spicules were preserved.[26] In this study, two obvious members can be recognized by changes in TOC, P/Al, Cu_{EF}, Ni_{EF}, and Cd/Mo in the Niutitang Formation (Figures 3 and 4). The lower member (LM, 0−23.5 m) shows high TOC (average 14.9%), P/Al (average 50.4×10^{-3}), Cu_{EF} (average 49.9), Ni_{EF} (average 49.9), and Cd/Mo (average 0.3437). The upper member (UM, 23.5−65 m) reveals moderate TOC (average 12.1%), P/Al (average 10.1×10^{-3}), Cu_{EF} (average 11.6), Ni_{EF} (average 8.2), and Cd/Mo (average 0.0663).

2.2. Stratigraphic Correlations for the Study Sections.

The stratigraphic correlations have been roughly established in the early Cambrian Nanhua Basin based on index fossils, lithostratigraphic markers, and U−Pb ages (Figure 2).[9] The Ediacaran/Cambrian boundary at ∼539 Ma lies at the top of the Dengying Formation based on extensive occurrences of the Basal Cambrian Carbon Isotope Excursion (BACE) in the Nanhua Basin and other areas globally.[27] This boundary is placed within the Liuchapo Formation based on (1) the appearances of small shelly fossils at Longbizui[28] and (2) a series of similar U−Pb ages, for example, 545.76 ± 0.66 Ma at Longbizui,[29] 542.6 ± 3.7 Ma at Bahuang,[30] and 541.48 ± 0.46 Ma at Pingying.[31]

The lithological change from dolostone or chert to black shale at the base of the Niutitang and Shuijingtuo formations has been taken as a correlation marker based on some similar U−Pb ages at the base of the organic-rich sequence, for example, 526.5 ± 1.1 Ma at Meishucun,[32] 526.43 ± 0.54 Ma at Yanjiahe,[33] 522.3 ± 3.7 Ma at Bahuang,[30] and 522.7 ± 4.9 Ma at Taoying.[34] The Ni−Mo layer has been regarded as another lithological marker for the boundary between Cambrian ages 2 and 3 (∼521 Ma), which is dated to 521 ± 5 Ma by Re−Os isotopes.[35]

An obvious drop in the TOC concentration is widely recognized in the middle Niutitang and Shuijingtuo formations (Figure 2). The TOC decline has been considered to be a correlation marker because it might respond to a fall in sea level in the Nanhua Basin. This stratigraphic correlation is supported by the appearances of the contemporary fossils in the Jinsha section, TZS drill core, and YJK drill core.[36] For example, *Zhenbaspis* at Jinsha and Qingjiang fossils at both TZS drill core and YJK drill core appear in the *Wutingaspis*−*Eoredlichia* Assemblage Zone.[37] The lithological shift from mudstone, silty shale, or shale to limestone at the end of the Niutitang Formation (or the upper Shuijingtuo Formation) has been taken as a correlation marker in the Nanhua Basin[6,9,38] because it might be in response to a continued marine regression.[9,38] This lithological transition is accompanied by a change in the trilobite zone from the *Wutingaspis*−*Eoredlichia* to *Yunnanaspis*−*Yiliangella* Assemblage Zone,[36] which is dated to 515.41 ± 1.91 Ma based on the cyclostratigraphic analysis.[39]

3. MATERIALS AND METHODS

A total of 47 samples were collected at Yuanjia for geochemical analyses. TOC, Al, redox proxies (Fe speciation, Mo_{EF}, and U_{EF}), and upwelling proxies (Co × Mn and Cd/Mo) were discussed in the previous studies.[14,40] Nutrient-related elements (P, Cu, and Ni) of 29 samples were analyzed in a previous study.[40] In this study, P for 17 new samples and Ti for all samples were conducted at the China University of Geosciences (Wuhan). Trace elements (Th, Cu, Ni, Ba, and Nd) and rare earth elements (REEs) were measured for 17 new samples at Nanjing FocuMS Technology Co.

For Ti and P analyses, approximately 0.6 mg of sample powder was weighed into a porcelain crucible. Approximately 6 g of $Li_2B_4O_7$ was added to the platinum crucible, which was well mixed with the sample powder by a porcelain spoon. The mixture was transferred into a platinum crucible, which was dissolved at 1080 °C. The platinum crucible was cooled to form a glass disk for Ti and P analyses using X-ray fluorescence (XRF) spectrometry. The long-term analyses of two standards (i.e., GBW07107 and GBW07108) yield an analytical error of less than 10%.

For nutrient elements and REEs, approximately 0.3 g of sample powder was heated at 150 °C for 12 h in order to remove volatiles. Approximately 50 mg of the dried sample was weighed into a Teflon bomb. Following the successive additions of 1 mL HNO_3 and 1 mL HF, the Teflon bomb was put into a steel sleeve, which was heated at 190 °C for above 24 h. The Teflon bomb was opened after cooling and was heated at 140 °C on a hot plate. When the solution was completely evaporated, 1 mL HNO_3 was added to the Teflon bomb. In order to make the solution entirely evaporate again, the Teflon bomb was heated at 140 °C. The Teflon bomb was put into a steel sleeve again with the successive additions of 1 mL HNO_3, 1 mL MQ water, and 1 mL ln, which was heated at 190 °C for above 12 h. The final solution was transferred to a polyethylene bottle, which was diluted to 100 g through 2% HNO_3. The diluted solution was analyzed using an Agilent 7500a quadrupole inductively coupled plasma mass spectrometer. The long-term tests of two standards (i.e., BCR-2 and GBW07108) produce an analytical error of less than 5%. Enrichment factors (EFs) are calculated as the ratios of elements to Al in samples compared to the average upper continental crust (AUCC), as $X_{EF} = (X/Al)_{sample}/(X/Al)_{AUCC}$, where X refers to the interested elements (e.g., Cu and Ni), and elemental values of AUCC are from McLennan.[41]

4. RESULTS

All geochemical data are listed in the Supporting Information, and the key proxies are summarized in Figures 3 and 4. In the study section, TOC exhibits a general decrease from the LM to the UM, varying between 6.4 and 35.5% (average 13.1%). Cu_{EF} ranges from 1.3 to 196 (average 24.4), which is high in the LM (8.6−196, average 49.9) compared to the UM (1.3−196, average 24.4). Ni_{EF} varies between 2.0 and 74.4 (average of 13.5), which shows a negative shift from the LM to the UM. P/Al declines from the LM to the UM, ranging from 1.7×10^{-3} to 256×10^{-3} (average 24.5×10^{-3}). Al ranges from 0.9 to 5.9% (average 3.6%), which is low in the LM (0.9−5.9%, average 2.9%) relative to the UM (2.2−5.4%, average 3.9%). Th varies between 2.7 and 8.5% (average 6.2%), which is low in the LM

https://doi.org/10.1021/acsomega.3c09161
ACS Omega 2024, 9, 19892−19903

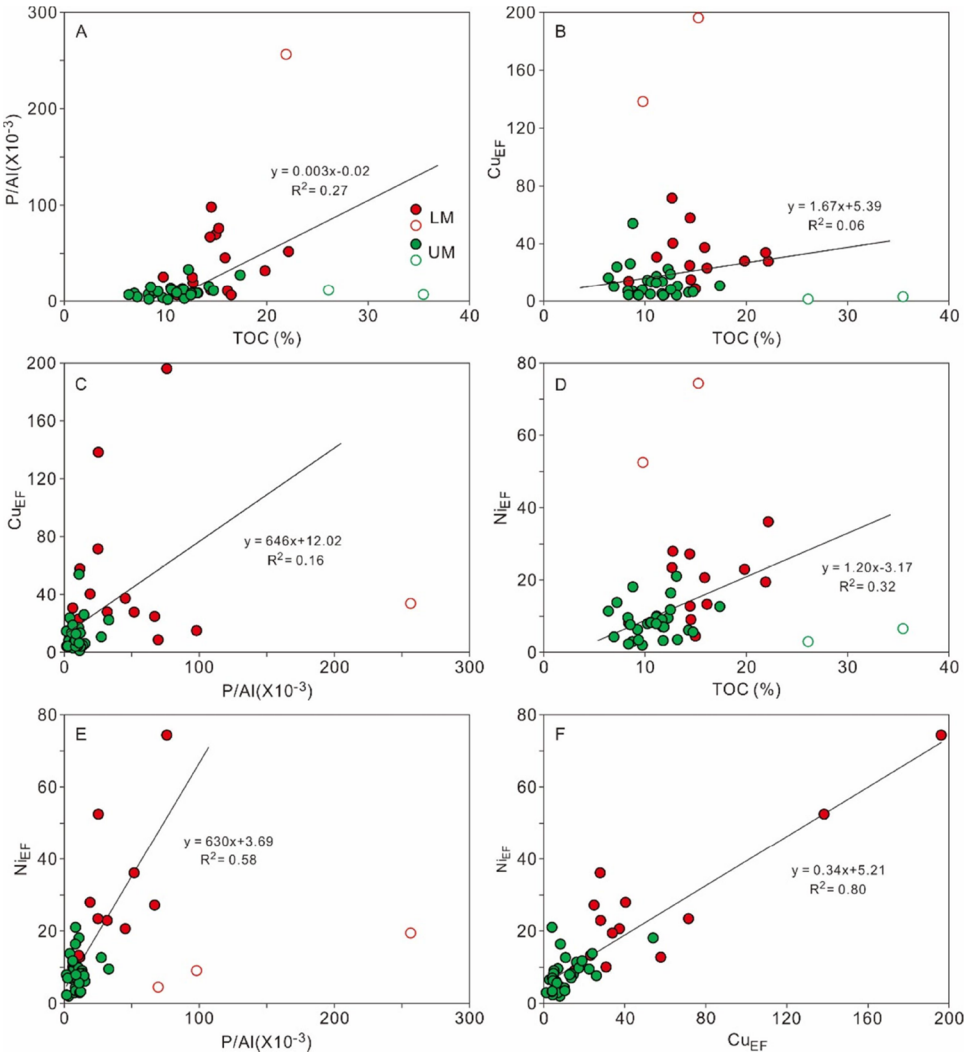

Figure 5. TOC versus P/Al (A) and Cu_{EF} (B), P/Al versus Cu_{EF} (C), TOC versus Ni_{EF} (D), P/Al versus Ni_{EF} (E), and Cu_{EF} versus Ni_{EF} (F) in the Yuanjia section.

(2.7−8.5%, average 4.9%) compared to the UM (4.1−8.4%, average 6.7%). Al/(Al+Fe+Mn) ranges from 0.40 to 0.93 (average 0.61), which shows a slight increase from the LM to the UM. Fe/Ti varies between 0.60 and 18.1 (average 8.88), which increases from the LM to the UM. Eu/Eu* is stable from the LM to the UM, ranging from 0.89 to 1.46 (average 1.05). Ce/Ce*varies between 0.38 and 1.04 (average 0.74). Y/Y* ranges from 1.15 to 1.75 (average of 1.47).

5. DISCUSSION

5.1. Reconstruction for Marine Productivity in the Early Cambrian Nanhua Basin. *5.1.1. Productivity Proxies.* TOC is frequently used to evaluate marine productivity owing to its direct relationship with primary producers.[42] In the photic zone, primary producers absorb carbon dioxide to yield organic matter through photosynthesis. A part of the organic matter in the photic zone is consumed by producer respiration and animal predation, and the rest is sunk into the deep ocean. In general, a majority of organic matter is degraded through bacterial respiration from the surface ocean to the sediment−water interface,[43] causing a small portion of organic matter to reach the sediment.[44] The residual organic matter is substantially consumed by diagenetic processes, which can be preserved in the sedimentary rock.[45] Therefore, the analyzed TOC values might be affected by other factors (e.g., detrital dilution, redox conditions, and sedimentation rates) except for marine productivity.[46] Strong detrital input can dilute organic matter in the sediment.[6] Organic matter tends to be well preserved in reducing conditions rather than under oxic conditions, which is because of the substantial loss through aerobic relative to anaerobic respiration.[42] Rapid sedimentation accelerates the isolation of organic matter from the oxic seawater or porewater, enhancing the preservation of organic matter.[47]

As a nutrient element, P is taken as an effective productivity proxy.[48] P is an indispensable nutrient for the growth of marine phytoplankton, which is an important composition of each organism. It is sunk to the sediment−water interface with organic remains after the death of organisms, and thus, P in the sediment is strongly associated with marine productivity in the surface ocean.[42] The fate of P in the sediment is primarily controlled by bottomwater redox conditions. In oxic states, P released via the remineralization of organic matter is adsorbed onto Fe-oxyhydroxides or biologically sequestrated into polyphosphates.[49] In reducing states, Fe-oxyhydroxides are dissolved.[50] For these reasons, under reducing conditions, P is

https://doi.org/10.1021/acsomega.3c09161
ACS Omega 2024, 9, 19892−19903

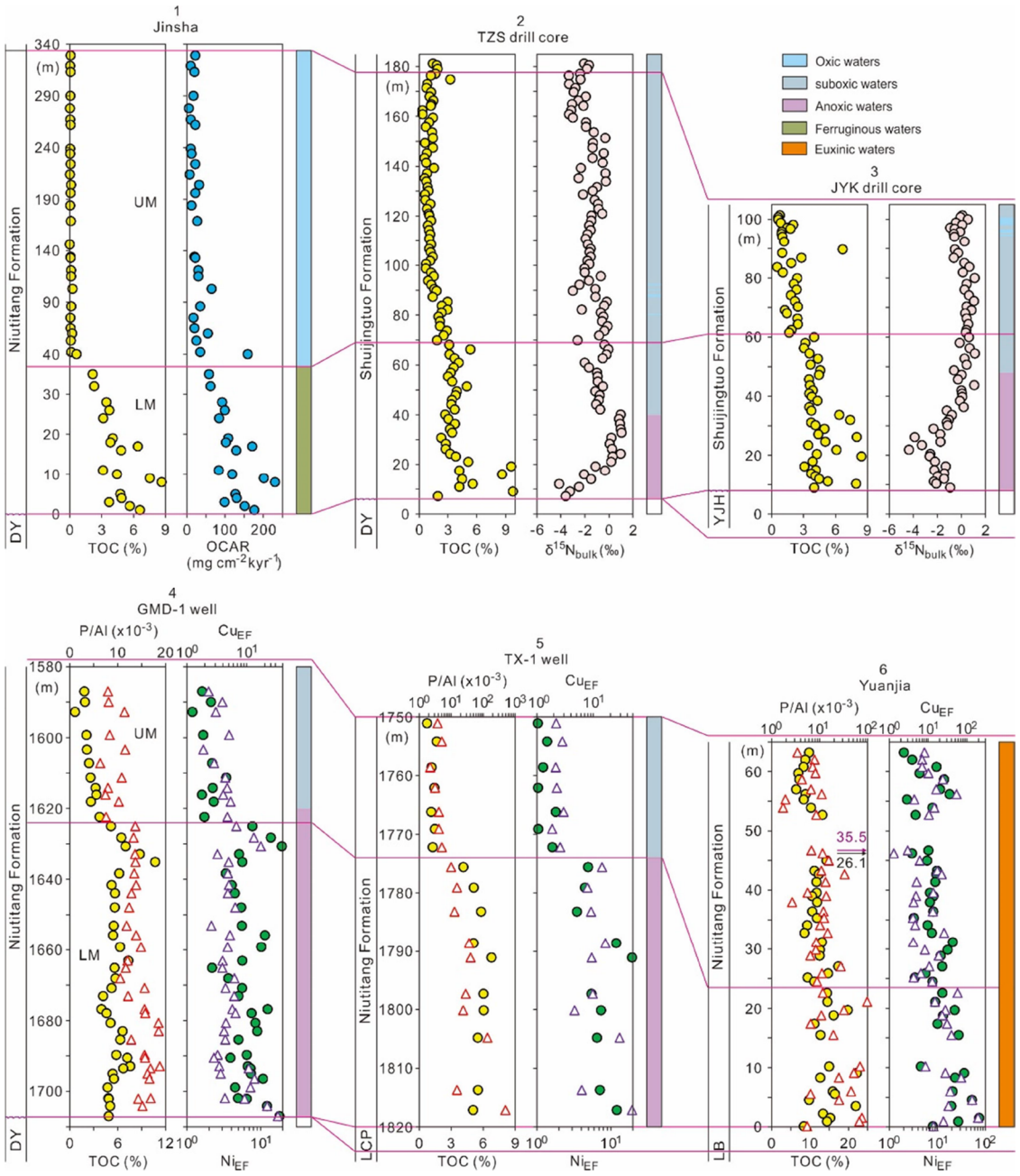

Figure 6. Comparisons of marine productivity in the Yuanjia section to other sections in the Nanhua Basin. Productivity and redox sources: 1—Jinsha,[6] 2—TZS drill core,[12] 3—JYK drill core,[12] 4—GDM-1 well,[16] 5—TX-1 well,[16] and 6—Yuanjia (this study).

generally released from the sediments to the overlying water columns.

As micronutrient elements, Cu and Ni are usually applied to evaluate primary productivity.[51,52] Cu and Ni are absorbed by organisms to yield organic matter along with the photosynthesis, and they have a good relationship with organic matter in the surface ocean.[53] However, Cu and Ni are also profoundly affected by the water-column redox conditions. Under oxic conditions, a majority of Cu exists in the form of organic−metal ligands, and the rest is present as $CuCl^+$.[49] Cu is retained in the sediment through both processes of adsorption onto Fe−Mn-oxyhydroxides and complexation with organic matter.[54] Under anoxic conditions, Cu^{2+} is reduced to Cu^+, which is deposited as CuS, Cu_2S, or incorporated in FeS_2.[49] In oxic states, Ni exists as Ni^{2+} or $NiCl^+$.[54] It is retained in the sediment through the complexation with organic matter. In mildly reducing states, Ni can diffuse from the sediments to the overlying seawaters owing to the lack of Mn oxides and sulfides.[49] In strong reducing states, Ni is precipitated as NiS.[55]

5.1.2. Primary Productivity at Yuanjia. The productivity proxies can be significantly affected by local water-column redox conditions (see Section 5.1.1). Accordingly, local redox states should be taken into consideration before the exploration of the primary productivity. Fe speciation (i.e., Fe_{HR}/Fe_T and Fe_{py}/Fe_{HR}) and redox-sensitive elements (i.e., Mo_{EF} and U_{EF}) suggest persistently euxinic conditions at Yuanjia (Figure 3).[14] The relatively stable redox conditions are accompanied by the general decreases in productivity proxies from the LM to the UM (Figure 3), suggesting that local redox conditions play minor roles in the fluctuations of the productivity proxies.

https://doi.org/10.1021/acsomega.3c09161
ACS Omega 2024, 9, 19892−19903

The covariations in TOC and P/Al are usually applied to distinguish redox and productivity effects. In redox-dominated systems, TOC is generally negatively correlated with P/Al, which mainly reflects their reverse behaviors under reducing conditions.[42] In contrast, TOC tends to show a positive correlation with P/Al in productivity-dominated systems because they are commonly controlled by marine productivity.[42] In the Yuanjia section, a weakly positive relationship between TOC and P/Al may indicate that marine productivity is first-order control on their variations (R^2 = 0.27; Figure 5A). Therefore, the generally downward trends in the TOC and P/Al record a long-term decrease in marine productivity from the LM to the UM at Yuanjia (Figure 3).

Micronutrients (Cu and Ni) can track marine productivity based on their relationships with TOC and P/Al. In the Yuanjia section, the TOC shows no correlation with Cu_{EF} (R^2 = 0.06; Figure 5B), suggesting that Cu accumulation is not directly controlled by sedimentary organic matter. P/Al exhibits a slightly positive relationship with Cu_{EF} (R^2 = 0.16; Figure 5C), implying that marine productivity has significant effects on Cu accumulation. The weakly positive correlation between TOC and Ni_{EF} (R^2 = 0.32; Figure 5D) is indicative of productivity control on Ni accumulation, which is consistent with the moderately positive relationship between P/Al and Ni_{EF} (R^2 = 0.58; Figure 5E). A strong positive correlation is recorded between Cu_{EF} and Ni_{EF} (R^2 = 0.80; Figure 5F), given that they are mainly associated with marine productivity. For these reasons, the reduced TOC, P/Al, Cu_{EF}, and Ni_{EF} point to a decline in marine productivity from the LM to the UM (Figure 3).

5.1.3. Marine Productivity at Other Coeval Sections in the Nanhua Basin. To reconstruct marine productivity at a broader scale, previously reported productivity results from the outer-shelf Jinsha section,[6] TZS drill core,[12] YJK drill core,[12] GMD-1 well,[16] and slope TX-1 well[16] are compiled (Figure 6). These data provide a potential to evaluate the temporal changes in marine productivity across the early Cambrian Nanhua Basin. Different proxies are used to explore marine productivity of the compiled sections because of the data availability, i.e., TOC and organic carbon accumulation rate (OCAR) at Jinsha,[6] TOC and $\delta^{15}N_{TN}$ in TZS and YJK drill cores,[12] TOC, P/Al, Cu_{EF}, and Ni_{EF} in GMD-1 and TX-1 wells[16] (Figure 6). It should be noted that OCAR is frequently used to assess marine productivity because of their positive relationship in modern oceans.[42] Sedimentary $\delta^{15}N_{TN}$ data can possibly trace marine productivity owing to its strong connection with marine nitrogen cycle.[12]

In the Jinsha section, the LM exhibits high productivity on the basis of elevated TOC (2.2−8.6%, average 4.6%) and OCAR (57.9−230 mg cm^{-2} kyr^{-1}, average 123 mg cm^{-2} kyr^{-1}), but the UM shows low productivity according to negligible TOC (0−0.6%, average 0.1%) and OCAR (5.0−158 mg cm^{-2} kyr^{-1}, average 28.2 mg cm^{-2} kyr^{-1}).[6] Therefore, the TOC and OCAR suggest a fall in marine productivity from the LM to the UM.

In the TZS drill core, the LM is characterized by high TOC (2.0−9.8%, average 4.1%) and low $\delta^{15}N_{TN}$ (−4.2 to +1.0 ‰, average −0.7 ‰), whereas the UM reveals low TOC (0.3−3.3%, average 1.3%) and $\delta^{15}N_{TN}$ (−3.3 to −0.1‰, average −1.6‰).[12] In the YJK drill core, the LM shows high TOC (3.0−8.4%, average 4.5%) and low $\delta^{15}N_{TN}$ (−4.4 to +1.1‰, average −1.1‰), but the UM exhibits low TOC (0.5−6.7%, average 1.7%) and $\delta^{15}N_{TN}$ (−0.9 to +1.1‰, average 0.2‰).[12] In both TZS and YJK drill cores, low $\delta^{15}N_{TN}$ data of anoxic samples in the LM suggest that the marine nitrogen cycle is dominated by quantitative assimilation of upwelled NH_4^+ and intense nitrogen fixation, which results from expansions of anoxic waters into the photic zone. The developments of widespread anoxic conditions are driven by elevated marine productivity as evidenced by high TOC. On the contrary, low $\delta^{15}N_{TN}$ data of oxic−suboxic samples in the UM suggest that the marine nitrogen cycle is dominated by biological N_2 fixation, which is caused by the limited nitrate availability in association with low marine productivity based on low TOC. In summary, TOC and $\delta^{15}N_{TN}$ suggest a decrease in marine productivity from the LM to the UM.

In the GDM-1 and TX-1 wells, TOC, P/Al, Cu_{EF}, and Ni_{EF} can reflect changes in marine productivity according to their positive covariations, which are similar to those in the Yuanjia section (Figure 6). In the GDM-1 well, the LM exhibits high productivity based on elevated TOC (4.0−10.7%, average 5.9%), P/Al (10.6×10^{-3}−46.1×10^{-3}, average 16.5×10^{-3}), Cu_{EF} (2.6−33.2, average 7.5), and Ni_{EF} (2.2−19.3, average 7.6), but the UM reveals low productivity as documented by low TOC (0.7−3.7%, average 2.4%), P/Al (6.3×10^{-3}−11.5×10^{-3}, average 8.9×10^{-3}), Cu_{EF} (1.9−5.4, average 3.9), and Ni_{EF} (0.8−3.4, average 1.9).[16] In the TX-1 well, the LM shows high productivity according to elevated TOC (4.1−6.8%, average 5.5%), P/Al (10.0×10^{-3}−494×10^{-3}, average 81.2×10^{-3}), Cu_{EF} (4.6−48.3, average 15.5), and Ni_{EF} (3.5−19.5, average 8.3), but the UM reveals low productivity on the basis of low TOC (0.7−1.7%, average 1.3%), P/Al (2.2×10^{-3}−5.1×10^{-3}, average 3.9×10^{-3}), Cu_{EF} (1.9−3.0, average 2.4), and Ni_{EF} (1.0−1.8, average 1.3).[16] In short, the decreases in TOC, P/Al, Cu_{EF}, and Ni_{EF} suggest a decrease in marine productivity from the LM to the UM.

5.2. Possible Factors Controlling Marine Productivity in the Early Cambrian Nanhua Basin. *5.2.1. Upwelling.* Cd and Cd/Mo are usually used to distinguish marine upwelling from restricted environments. Cd and Mo are, importantly, influenced by water-column redox conditions. Under oxic conditions, Cd and Mo are present as Cd^{2+} and molybdate (MoO_4^{2-}), respectively.[49] In the presence of H_2S, Cd is present in the form of CdS, and Mo forms particle-reactive thiomolybdates ($MoO_{4-x}S_x^{2-}$, x = 1−4).[54] On the other hand, Cd is also linked to marine productivity, which reveals a nutrient-type profile from surface to deep waters.[51] However, Mo is conservative in seawater, which exhibits an obvious contrast to nutrient-like elements (e.g., Cd).[56] Hence, the modern upwelling sediments show high Cd_{EF} as a consequence of a huge supply of plankton material in rich of Cd under elevated productivity,[57] which also exhibits elevated Cd/Mo owing to more effective fluxes of Cd to the sediments compared to Mo.[56] In contrast, the modern restricted environments reveal low Cd_{EF} and Cd/Mo because of the limited Cd availability and similar fluxes of Cd and Mo to the sediment, respectively.[56,57]

Co, Mn, and Co × Mn are frequently applied to assess marine upwelling and restricted environments. Co and Mn are associated with water-column redox conditions. Under oxic conditions, Co is soluble as Co^{2+}, but Mn is insoluble as Mn(III) or Mn(IV) hydroxides or oxides.[49] Under anoxic conditions, Co is present as CoS, and Mn is converted to Mn^{2+} or $MnCl^+$.[54] Co and Mn behaviors are different in marine upwelling and restricted environments. In upwelling environments, Co and Mn enrichments mainly depend on detrital minerals, which are generally depleted in deep waters.[56] Thus, the upwelling environments are characterized by low Co_{EF}, Mn_{EF}, and Co × Mn owing to the limited fluxes of Co and Mn from deep to

https://doi.org/10.1021/acsomega.3c09161
ACS Omega 2024, 9, 19892−19903

surface waters.[56,57] In restricted settings, the supplies of Co and Mn are mainly controlled by high riverine fluxes.[56] Hence, the restricted settings show high Co_{EF}, Mn_{EF}, and Co × Mn due to enough supplies of both Co and Mn from river waters.[56,57]

The upwelling proxies are significantly associated with water-column redox conditions, and thus, the redox effects should be explored prior to the applications of the upwelling proxies. Fe speciation and redox-sensitive elements suggest relatively stable redox states (i.e., persistently euxinic conditions) in the Yuanjia section (Figure 3). This redox variation is consistent with the decreased trends of Cd_{EF} and Mn_{EF} (Figure 4), suggesting that marine redox conditions have minor effects on changes in Cd_{EF} and Mn_{EF}. However, water-column redox conditions play key roles in Co_{EF} because of their similar changes (Figures 3 and 4), suggesting that Co_{EF} and Co × Mn are not valid to assess marine upwelling.

Our results suggest the weakened upwelling from the LM to the UM. In the LM, euxinic samples are characterized by high Cd_{EF} (37.2−3030, average 904) and low Mn_{EF} (0.01−0.92, average 0.23) (Figure 7), which have been discovered in modern

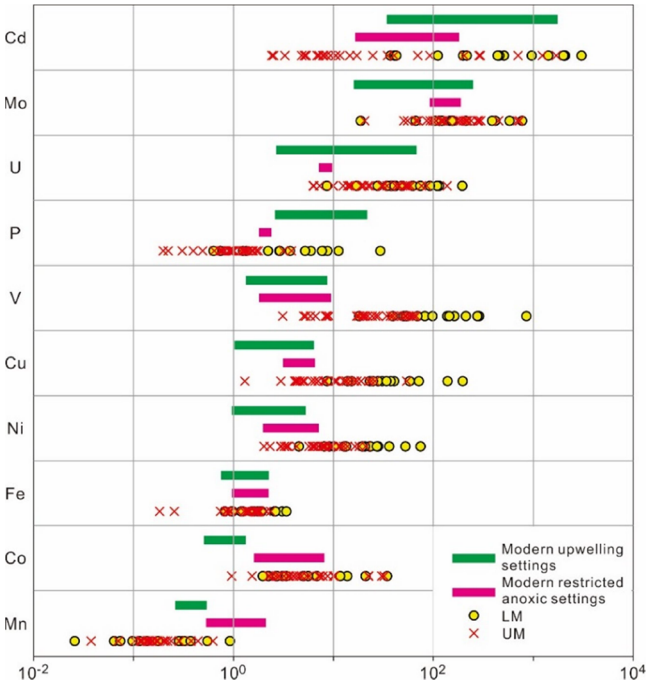

Figure 7. Patterns of elemental enrichments in the Yuanjia section. Elemental enrichments of costal upwelling environments and restricted environments are sourced from Brumsack.[57]

coastal upwelling environments instead of modern restricted environments.[54] Strong upwelling is supported by high Cd/Mo (0.0154−1.1885, average 0.3437) (Figure 4). In the UM, euxinic samples show moderate Cd_{EF} (2.4−1694, average 161) and low Mn_{EF} (0.04−0.62, average 0.18), suggesting weak upwelling (Figure 7). The reduced upwelling is supported by low Cd/Mo (0.005−0.7532, average 0.0663) (Figure 4).

The appearance of an upwelling system in the early Cambrian Nanhua Basin might be linked to paleogeographic and climatic conditions. The Nanhua Basin was suited in the low to midpaleolatitudes (0−30° N) of the northern hemisphere (Figure 1A). This range of paleolatitudes might allow the northeaster trade winds in the subtropical arid zone to develop in the Nanhua Basin, where the cool and arid climate is supported by low chemical index of alteration (CIA)[58] and high Ti/Al.[59] A rise of trade winds stimulates the developments of the oblique offshore currents, leading to the occurrence of extensive upwelling in the Nanhua Basin.[59]

5.2.2. Hydrothermal Activity. Al/(Al+Mn+Fe) and Fe/Ti are commonly applied to evaluate hydrothermal activity.[20] In general, elevated Fe and Mn are associated with hydrothermal activity, whereas high Al and Ti are attributed to terrigenous fluxes.[19] Hence, Al/(Al+Mn+Fe) < 0.4 and Fe/Ti > 20 are generally indicative of hydrothermal activity, but Al/(Al+Mn+Fe) > 0.4 and Fe/Ti < 20 usually point to terrigenous fluxes.[60,61] More visually, an Fe−Al−Mn ternary diagram can distinguish the hydrothermal and nonhydrothermal origins.[62]

The REE pattern is another effective proxy to track hydrothermal activity. Hydrothermal fluids show depletion in heavy REEs (HREEs), positive Eu anomaly, and negligible negative Ce anomaly.[63] In contrast, REE patterns of seawaters are characterized by enrichment in HREEs, significantly negative Ce anomalies, no obvious Eu anomalies, and positive Y anomalies.[64,65] Positive Eu anomaly can be caused by the Ba interference during analysis, which can be tracked by the relationship between Ba/Nd and Eu anomalies.[66,67]

In this study, all samples are characterized by high Al/(Al+Mn+Fe) (0.40−0.93, average 0.61) and low Fe/Ti (0.60−18.11, average 8.67) (Figure 4), suggesting a minor influence from hydrothermal input. This explanation is consistent with a Fe−Al−Mn ternary diagram indicative of nonhydrothermal activities (Figure 8). All samples show seawater-like REE

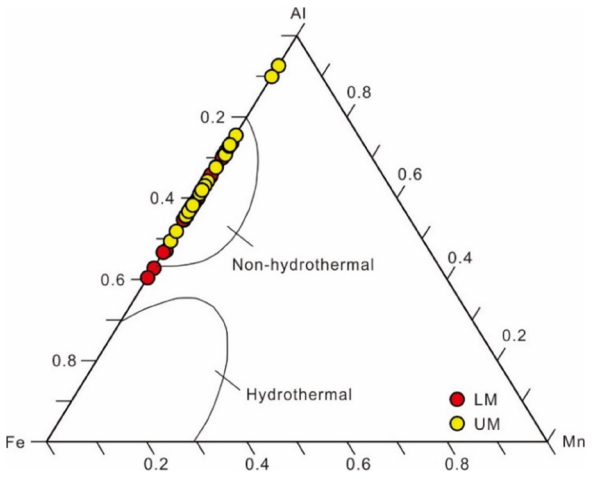

Figure 8. Al−Fe−Mn ternary diagram in the Yuanjia section. The distinguish between hydrothermal and nonhydrothermal origins is according to Yamamoto.[62]

patterns, as suggested by enrichment in HREE, negative Ce anomalies (0.38−1.04, average 0.74), and positive Y anomalies (1.15−1.75, average 1.47) (Figure 9). Given the weakly positive correlation between Ba/Nd and Eu/Eu* (R^2 = 0.29; Figure 10), the positive Eu anomalies (up to 1.46) of some samples might be affected by Ba interference. In summary, there are almost no hydrothermal fluids in the study section.

5.2.3. Terrigenous Input. Al and Th are frequently used to assess local terrigenous fluxes in marine systems. Al and Th are insoluble in seawater, which are immobile during chemical weathering and diagenesis.[68] In this study, the moderately positive correlation between Al and Th (R^2 = 0.74) suggests that both Al and Th are mainly controlled by terrigenous inputs

https://doi.org/10.1021/acsomega.3c09161
ACS Omega 2024, 9, 19892−19903

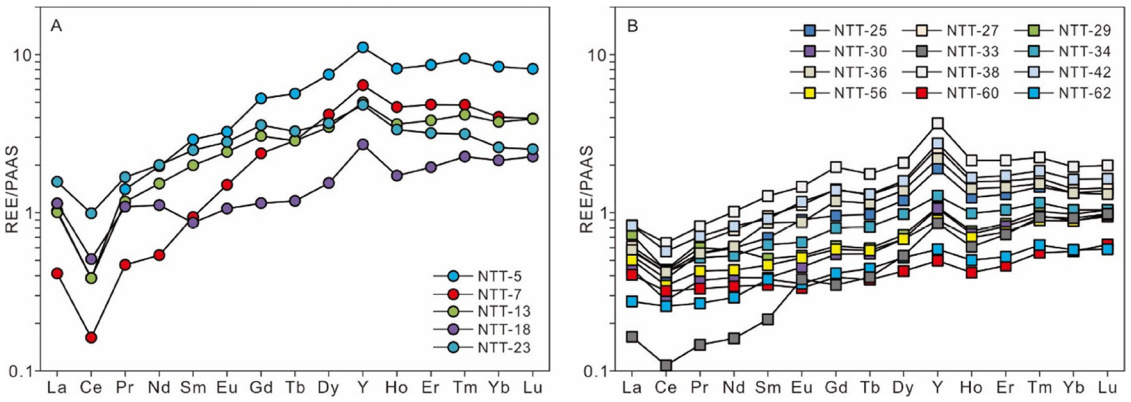

Figure 9. PAAS-normalized REE patterns are in the Yuanjia section.

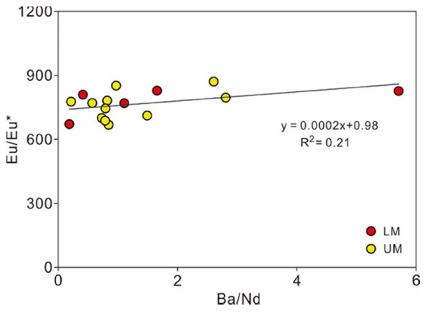

Figure 10. Cross plot of Ba/Nd versus Eu*/Eu in the Yuanjia section.

(Figures 4 and 11). Our samples show low Al (0.9−5.9%, average 2.9%) and Th (2.7−8.5 ppm, average 4.9 ppm) in the

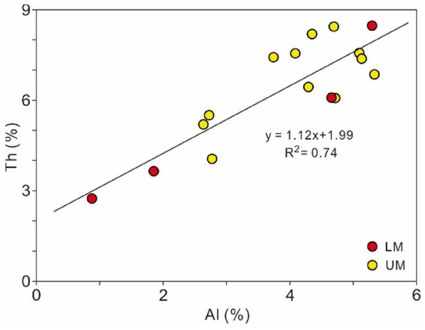

Figure 11. Cross plot of Al vs Th in the Yuanjia section.

LM, reflecting low terrigenous fluxes. Our samples reveal high Al (2.2−5.4%, average 3.9%) and Th (4.1−8.4 ppm, average 6.7 ppm) in the UM, pointing to high terrigenous fluxes. The enhanced terrigenous fluxes from the LM to the UM possibly result from an increase in continental erosion as indicated by $^{87}Sr/^{86}Sr$ values at the same time.[69]

5.3. Drivers of the Decreased Marine Productivity in the Nanhua Basin. Changes in marine productivity are generally assumed to be controlled by terrigenous fluxes, where high marine productivity is connected with elevated fluxes of terrigenous nutrients.[70,71] Nevertheless, our result of decreased marine productivity is consistent with the enhanced terrigenous fluxes in the Nanhua Basin from late age 2 to late age 3 (~526−515 Ma), which does not support the terrigenous controls on marine productivity (Figures 3 and 4).

Fluctuations in marine productivity are considered to be caused by hydrothermal activities.[16,17] Hydrothermal fluids can release a large number of nutrients, resulting in high marine productivity.[72] Thus, marine productivity is expected to be higher in the hydrothermal active areas than in other normal sections. For example, marine productivity based on TOC contents is high near the hydrothermal active area (e.g., Tongren section) relative to nonhydrothermal sections in the Nanhua Basin.[17] However, our finding of low TOC values (average 1.4%) at Tongren and high TOC values (average 13.1%) at Yuanjia do not support a significant influence of hydrothermal activities on marine productivity, where hydrothermal and nonhydrothermal activities are recognized in the Tongren[17] and Yuanjia sections (this study), respectively. This inference is in agreement with the existence of a decrease in marine productivity in nonhydrothermal areas (e.g., Yuanjia section; this study).

Variations in marine productivity are supposed to be contributed to upwelling.[6,14,40] Strong upwelling can bring massive nutrients from the deep ocean to the photic zone of shallow waters, leading to high marine productivity. In contrast, the diminished upwelling weakens nutrient availability from deep waters to surface waters, resulting in low marine productivity. This significant effect of upwelling on marine productivity is evidenced by the good relationship between them in this study. For example, high marine productivity and strong upwelling appear simultaneously in the LM, but low marine productivity coexists with diminished upwelling in the UM (see Sections 5.1.3 and 5.2.1).

5.4. Implications for the Animal Radiations during the Early Cambrian. The Cambrian explosion is known for the first appearance of metazoan phyla and the establishment of a complex marine ecosystem dominated by metazoans during the early Cambrian. During Fortunian and age 2, the evolution of early animals is represented by the occurrence of small shelly fauna globally.[1,2] In the transition from late age 2 to early age 3 (~526−518 Ma), small shelly fauna is replaced by panarthropods in the inner-shelf settings of the Nanhua Basin, but Niutitang sponge fauna dominated by sponges appears from outer shelf to slope to basinal settings.[2,73] In late age 3 (~518−514 Ma), the Cambrian explosion reached its peak as evidenced by the appearances of Chengjiang and Qingjiang biotas.[2,37]

Our reconstruction of marine productivity provides an opportunity to explore its relationship with metazoan evolution during the early Cambrian. Our results show a decreased marine productivity from late age 2 to age 3 (Figure 6), while the evolution of life exhibits an increase in metazoan complexity and diversity.[2,37] The reverse trends of marine productivity and metazoan evolution suggest that food was not a major factor

https://doi.org/10.1021/acsomega.3c09161
ACS Omega 2024, 9, 19892−19903

controlling the evolution of early animals during the Cambrian explosion. Such an inference conforms to no direct relationships between marine productivity and the occurrences of early animals (e.g., Niutitang sponge fauna and Qingjiang Biota). In the modern ocean, sponges can thrive in an oligotrophic environment because they can uptake dissolved organic matter and nutrients from the surrounding seawater.[74] However, Niutitang sponge fauna appears in high-productivity environments based on high OCAR at Jinsha[6] and ε^{112}Cd at Zunyi.[75] It is well accepted that a large amount of foods are needed for microphagous suspension feeders.[76] For example, modern whales, whale sharks, and basking sharks live in high latitudes with elevated marine productivity.[77] Nevertheless, Qingjiang biota occurs in an oligotrophic environment based on $\delta^{15}N_{TN}$ in both TZS and YJK drill cores.[12]

Marine productivity might stimulate the radiation of early animals through its effect on atmospheric-oceanic oxygen levels. Low marine productivity inhibits organic matter burial, resulting in low oxygen levels in the atmosphere-ocean system. In contrast, high marine productivity enhances organic matter burial, and thus, a huge amount of O_2 is released into the atmosphere, causing the oxygenation of the oceanic systems. The significant effect of high marine productivity on oceanic oxygen levels is evidenced by episodes of oceanic oxygenation events based on U and Mo isotopes in the LM.[78,79] Correspondingly, the Niutitang sponge fauna widely appears in the Nanhua Basin. On the other hand, low marine productivity reduces water-column oxygen consumption, leading to local oxic conditions. The important influence of low marine productivity on redox conditions is documented by an expansion of local oxic conditions in the UM. As a consequence, complex faunas such as Chengjiang and Qingjiang biotas appear in the shelf areas of the Nanhua Basin.[9]

6. CONCLUSIONS

TOC, major, and trace elements were measured and compiled at Yuanjia to investigate changes in primary productivity and its relationship with the radiation of early animals in the early Cambrian. Our finding of synchronous changes in TOC, P/Al, Cu_{EF}, and Ni_{EF} suggests that they were effective to reconstruct marine productivity in the early Cambrian Nanhua Basin. Cd_{EF} and Cd/Mo can be regarded as the solid upwelling proxies in the Nanhua Basin owing to the significant effects of plankton biomass and redox conditions on Cd and Mo enrichments, respectively. Co_{EF} and Co × Mn failed to assess marine upwelling in the Nanhua Basin because Co enrichments were controlled by water-column redox conditions. Integrated with the existing productivity data from the outer shelf (Jinsha, TZS drill core, YJK drill core, and GDM-1 well) and slope areas (TX-1 well), our study reflects a decreased marine productivity from Age 2 to Age 3 in the Nanhua Basin. The decline in marine productivity was accompanied by weakened upwelling, quiet hydrothermal activity, and enhanced local terrestrial flux, suggesting that fluctuations in marine productivity might be mainly connected with upwelling. In comparison to fossil distributions, our study suggests that there might be enough food for the radiation of early animals in the early Cambrian Nanhua Basin. Marine productivity might indirectly trigger animal complexity and diversity by regulating water-column oxygen levels in the early Cambrian Nanhua Basin.

■ ASSOCIATED CONTENT

Supporting Information

The Supporting Information is available free of charge at https://pubs.acs.org/doi/10.1021/acsomega.3c09161.

Geochemical data in the Yuanjia section (PDF)

■ AUTHOR INFORMATION

Corresponding Authors

Chengsheng Jin − *College of Resource Environment and Tourism, Hubei University of Arts and Science, Xiangyang 441053, China*; orcid.org/0000-0002-8553-8103; Email: jchengshxsm@163.com

Tao Zhang − *College of Resource Environment and Tourism, Hubei University of Arts and Science, Xiangyang 441053, China*; Email: 2486510470@qq.com

Authors

Zihu Zhang − *State Key Laboratory of Oil and Gas Reservoir Geology and Exploitation & Institute of Sedimentary Geology, Chengdu University of Technology, Chengdu 610059, China*

Meng Cheng − *State Key Laboratory of Oil and Gas Reservoir Geology and Exploitation & Institute of Sedimentary Geology, Chengdu University of Technology, Chengdu 610059, China*

Guochang Wang − *Yunnan Key Laboratory for Palaeobiology, Institute of Palaeontology, Yunnan University, Kunming, Yunnan 650091, China*

Huajin Chang − *College of Resource Environment and Tourism, Hubei University of Arts and Science, Xiangyang 441053, China*

Zhengqi Cao − *College of Resource Environment and Tourism, Hubei University of Arts and Science, Xiangyang 441053, China*

Complete contact information is available at: https://pubs.acs.org/10.1021/acsomega.3c09161

Notes

The authors declare no competing financial interest.

■ ACKNOWLEDGMENTS

This study was supported by the NSFC Program (41902027, 41903032, and 42002027).

■ REFERENCES

(1) Zhang, X.; Shu, D.; Han, J.; Zhang, Z.; Liu, J.; Fu, D. Triggers for the Cambrian explosion: hypotheses and problems. *Gondwana Res.* **2014**, *25*, 896−909.

(2) Zhu, M.; Zhao, F.; Yin, Z.; Zeng, H.; Li, G. The Cambrian explosion: advances and perspectives from China. *Sci. China Earth Sci.* **2019**, *49*, 1455−1490.

(3) Sperling, E. A.; Frieder, C. A.; Raman, A. V.; Girguis, P. R.; Levin, L. A.; Knoll, A. H. Oxygen, ecology, and the Cambrian radiation of animals. *Proc. Natl. Acad. Sci. U. S. A.* **2013**, *110*, 13446−13451.

(4) Butterfield, N. J. Macroevolution and macroecology through deep time. *Palaeontology* **2007**, *50*, 41−55.

(5) Sperling, E. A.; Stockey, R. G. The temporal and environmental context of early animal evolution: Considering all the ingredients of an "explosion. *Integr. Comp. Biol.* **2018**, *58*, 605−622.

(6) Jin, C. S.; Li, C.; Algeo, T. J.; Wu, S. Y.; Cheng, M.; Zhang, Z. H.; Shi, W. Controls on organic matter accumulation on the early-Cambrian western Yangtze Platform. *South China. Mar. Pet. Geol.* **2020**, *111*, 75−87.

(7) Algeo, T. J.; Ingall, E. Sedimentary C_{org}:P ratios, paleocean ventilation, and Phanerozoic atmospheric pO_2. *Palaeogeogr., Palaeoclimatol., Palaeoecol.* **2007**, *256*, 130−155.

(8) Chen, X.; Ling, H. F.; Vance, D.; Shields-zhou, G. A.; Zhu, M. Y.; Poulton, S. W.; Och, L. M.; Jiang, S. Y.; Li, D.; Cremonese, L.; Archer, C. Rise to modern levels of ocean oxygenation coincided with the Cambrian radiation of animals. *Nat. Commun.* **2015**, *6*, 7142.
(9) Jin, C. S.; Li, C.; Algeo, T. J.; Planavsky, N. J.; Cui, H.; Yang, X. L.; Zhao, Y. L.; Zhang, X. L.; Xie, S. C. A highly redox-heterogeneous ocean in South China during the early Cambrian (~529−514 Ma): Implications for biota-environment co-evolution. *Earth Planet. Sci. Lett.* **2016**, *441*, 38−51.
(10) Stolper, D. A.; Keller, C. B. A record of deep-ocean dissolved O_2 from the oxidation state of iron in submarine basalts. *Nature* **2018**, *553*, 323−327.
(11) Wang, D.; Ling, H. F.; Struck, U.; Zhu, X. K.; Zhu, M. Y.; He, T. C.; Yang, B.; Gamper, A.; Shields, G. A. Coupling of ocean redox and animal evolution during the Ediacaran−Cambrian transition. *Nat. Commun.* **2018**, *9*, 2575.
(12) Chang, C.; Wang, Z.; Huang, K. J.; Yun, H.; Zhang, X. Nitrogen cycling during the peak Cambrian explosion. *Geochim. Cosmochim. Acta* **2022**, *336*, 50−61.
(13) Peters, S. E.; Gaines, R. R. Formation of the 'Great Unconformity' as a trigger for the Cambrian explosion. *Nature* **2012**, *484*, 363−366.
(14) Chen, Z.; Wang, G.; Jin, C. Marine redox variation and hydrographic restriction in the early Cambrian Nanhua Basin, South China. *Palaeogeogr., Palaeoclimatol., Palaeoecol.* **2022**, *607*, 111263.
(15) Liu, Z.; Yan, D.; Yuan, D.; Niu, X.; Fu, H. Multiple controls on the organic matter accumulation in early Cambrian marine black shales, middle Yangtze Block, South China. *J. Nat. Gas Sci. Eng.* **2022**, *100*, 104454.
(16) Wu, Y.; Tian, H.; Gong, D.; Li, T.; Zhou, Q. Paleo-environmental variation and its control on organic matter enrichment of black shales from shallow shelf to slope regions on the Upper Yangtze Platform during Cambrian Stage 3. *Palaeogeogr., Palaeoclimatol., Palaeoecol* **2020**, *545*, 109653.
(17) Zhu, G.; Wang, P.; Li, T.; Zhao, K.; Zheng, W.; Feng, X.; Shen, J.; Grasby, S. E.; Sun, G.; Tang, S.; Yan, H. Mercury record of intense hydrothermal activity during the early Cambrian, South China. *Palaeogeogr., Palaeoclimatol., Palaeoecol.* **2021**, *568*, 110294.
(18) Steiner, M.; Wallis, E.; Erdtmann, B. D.; Zhao, Y.; Yang, R. Submarine-hydrothermal exhalative ore layers in black shales from South China and associated fossils—insights into a Lower Cambrian facies and bio-evolution. *Palaeogeogr., Palaeoclimatol., Palaeoecol.* **2001**, *169*, 165−191.
(19) Liu, Z. H.; Zhuang, X. G.; Teng, G. E.; Xie, X. M.; Yin, L. M.; Bian, L. Z.; Feng, Q. L.; Algeo, T. J. The lower Cambrian Niutitang Formation at Yantiao (Guizhou, SW China): organic matter enrichment, source rock potential, and hydrothermal influences. *J. Petrol. Geol.* **2015**, *38*, 411−432.
(20) Xie, X.; Zhu, G.; Wang, Y. The influence of syngenetic hydrothermal silica fluid on organic matter preservation in lower Cambrian Niutitang Formation. *South China. Mar. Pet. Geol.* **2021**, *129*, 105098.
(21) Wang, Z.; Tan, J.; Boyle, R.; Hilton, J.; Ma, Z.; Wang, W.; Lyu, Q.; Kang, X.; Luo, W. Evaluating episodic hydrothermal activity in South China during the early Cambrian: Implications for biotic evolution. *Mar. Pet. Geol.* **2020**, *117*, 104355.
(22) Zhang, S.; Evans, D. A. D.; Li, H.; Wu, H.; Jiang, G.; Dong, J.; Zhao, Q.; Raub, T. D.; Yang, T. Paleomagnetism of the late Cryogenian Nantuo Formation and paleogeographic implications for the South China Block. *J. Asian Earth Sci.* **2013**, *72*, 164−177.
(23) Yang, B.; Steiner, M.; Keupp, H. Early Cambrian palaeobiogeography of the Zhenba−Fangxian Block (South China): Independent terrane or part of the Yangtze Platform? *Gondwana Res.* **2015**, *28*, 1543−1565.
(24) Goldberg, T.; Strauss, H.; Guo, Q.; Liu, C. Reconstructing marine redox conditions for the Early Cambrian Yangtze Platform: evidence from biogenic sulphur and organic carbon isotopes. *Palaeogeogr., Palaeoclimatol., Palaeoecol.* **2007**, *254*, 175−193.
(25) Jiang, G. Q.; Wang, X. Q.; Shi, X. Y.; Xiao, S. H.; Zhang, S. H.; Dong, J. The origin of decoupled carbonate and organic carbon isotope signatures in the early Cambrian (ca. 542−520 Ma) Yangtze platform. *Earth Planet. Sci. Lett.* **2012**, *317−318*, 96−110.
(26) Qin, Z.; Xu, D.; Kendall, B.; Zhang, X.; Ou, Q.; Wang, X.; Li, J.; Liu, J. Molybdenum isotope-based redox deviation driven by continental margin euxinia during the early Cambrian. *Geochim. Cosmochim. Acta* **2022**, *325*, 152−169.
(27) Zhu, M. Y.; Yang, A. H.; Yuan, J. L.; Li, G. X.; Zhang, J. M.; Zhao, F. C.; Ahn, S. Y.; Miao, L. Y. Cambrian integrative stratigraphy and timescale of China. *Sci. China Earth Sci.* **2019**, *62*, 25−60.
(28) Yi, Y.; Chen, F.; Algeo, T. J.; Feng, Q. Deep-water fossil assemblages from the Ediacaran−Cambrian transition of western Hunan, South China and their biostratigraphic and evolutionary implications. *Palaeogeogr., Palaeoclimatol., Palaeoecol.* **2022**, *591*, 110878.
(29) Yang, C.; Zhu, M. Y.; Condon, D. J.; Li, X. H. Geochronological constraints on stratigraphic correlation and oceanic oxygenation in Ediacaran-Cambrian transition in South China. *J. Asian Earth Sci.* **2017**, *140*, 75−81.
(30) Chen, D. Z.; Zhou, X. Q.; Fu, Y.; Wang, J. G.; Yan, D. T. New U−Pb zircon ages of the Ediacaran−Cambrian boundary strata in South China. *Terra Nova* **2015**, *27*, 62−68.
(31) Wang, W.; Zhou, M.; Chu, Z.; Xu, J.; Li, C.; Luo, T.; Guo, J. Constraints on the Ediacaran−Cambrian boundary in deep-water realm in South China: Evidence from zircon CA-ID-TIMS U-Pb ages from the topmost Liuchapo Formation. *Sci. China Earth Sci.* **2020**, *63*, 1176−1187.
(32) Compston, W.; Zhang, Z. C.; Cooper, J. A.; Ma, G. G.; Jenkins, R. J. F. Further SHRIMP geochronology on the early Cambrian of South China. *Am. J. Sci.* **2008**, *308*, 399−420.
(33) Yang, C.; Bowyer, F. T.; Condon, D. J.; Li, X. H.; Zhu, M. New U-Pb age from the Shuijingtuo Formation (Yangtze Gorges area) and its implications for the Cambrian timescale. *Palaeogeogr., Palaeoclimatol., Palaeoecol.* **2023**, *616*, 111477.
(34) Wang, X. Q.; Shi, X. Y.; Jiang, G. Q.; Zhang, W. H. New U−Pb age from the basal Niutitang Formation in South China: Implications for diachronous development and condensation of stratigraphic units across the Yangtze platform at the Ediacaran−Cambrian transition. *J. Asian Earth Sci.* **2012**, *48*, 1−8.
(35) Xu, L. G.; Lehmann, B.; Mao, J. W.; Qu, W. J.; Du, A. D. Re-Os age of polymetallic Ni-Mo-PGE-Au mineralization in early Cambrian black shales of South China—A reassessment. *Econ. Geol.* **2011**, *106*, 511−522.
(36) Yuan, J. L.; Zhao, Y. L. Subdivision and correlation of Lower Cambrian in southwest China, with a discussion of the age of Early Cambrian series biota. *Acta Palaeontol. Sin.* **1999**, *38*, 116−131.
(37) Fu, D.; Tong, G.; Dai, T.; Liu, W.; Yang, Y.; Zhang, Y.; Cui, L.; Li, L.; Yun, H.; Wu, Y.; Sun, A.; Liu, C.; Pei, W.; Gaines, R. R.; Zhang, X. The Qingjiang biota—a Burgess Shale−type fossil Lagerstätte from the early Cambrian of South China. *Science* **2019**, *363*, 1338−1342.
(38) Li, C.; Zhang, Z.; Jin, C.; Cheng, M.; Wang, H.; Huang, J.; Algeo, T. J. Spatiotemporal evolution and causes of marine euxinia in the early Cambrian Nanhua Basin (South China). *Palaeogeogr., Palaeoclimatol., Palaeoecol.* **2020**, *546*, 109676.
(39) Zhang, T.; Li, Y.; Fan, T.; Da silva, A. C.; Shi, J.; Gao, Q.; Kuang, M.; Liu, W.; Gao, Z.; Li, M. Orbitally-paced climate change in the early Cambrian and its implications for the history of the Solar System. *Earth Planet. Sci. Lett.* **2022**, *583*, 117420.
(40) Cheng, M.; Li, C.; Jin, C. S.; Wang, H. Y.; Algeo, T. J.; Lyons, T. W.; Zhang, F. F.; Anbar, A. Evidence for high organic carbon export to the early Cambrian seafloor. *Geochim. Cosmochim. Acta* **2020**, *287*, 125−140.
(41) Mclennan, S. M. Relationships between the trace element composition of sedimentary rocks and upper continental crust. *Geochem. Geophys. Geosyst.* **2001**, *2*, 203−236.
(42) Schoepfer, S. D.; Shen, J.; Wei, H.; Tyson, R. V.; Ingall, E.; Algeo, T. J. Total organic carbon, organic phosphorus, and biogenic barium

https://doi.org/10.1021/acsomega.3c09161
ACS Omega 2024, 9, 19892−19903

fluxes as proxies for paleomarine productivity. *Earth Sci. Rev.* **2015**, *149*, 23−52.
(43) Opsahl, S.; Benner, R. Distribution and cycling of terrigenous dissolved organic matter in the ocean. *Nature* **1997**, *386*, 480−482.
(44) Canfield, D. E. Factors influencing organic carbon preservation in marine sediments. *Chem. Geol.* **1994**, *114*, 315−329.
(45) Froelich, P. N.; Klinkhammer, G. P.; Bender, M. L.; Luedtke, G. R.; Heath, G. R.; Cullen, D.; Dauphin, P.; Hammond, D.; Hartman, B.; Maynard, V. Early oxidation of organic matter in pelagic sediments of the eastern equatorial Atlantic: suboxic diagenesis. *Geochim. Cosmochim. Acta* **1979**, *43*, 1075−1090.
(46) Zhang, K.; Liu, R.; Bai, E.; Zhao, Z.; Peyrotty, G.; Fathy, D.; Liu, Z. Biome responses to a hydroclimatic crisis in an early cretaceous (Barremian−Aptian) subtropical inland lake ecosystem, Northwest China. *Palaeogeogr. Palaeoclimatol. Palaeoecol.* **2023**, *622*, No. 111596.
(47) Fathy, D.; Wagreich, M.; Fathi, E.; Ahmed, M. S.; Leila, M.; Sami, M. Maastrichtian Anoxia and Its Influence on Organic Matter and Trace Metal Patterns in the Southern Tethys Realm of Egypt during Greenhouse Variability. *ACS Omega* **2023**, *8*, 19603−19612.
(48) Wang, H.; Zhang, Z.; Li, C.; Algeo, T. J.; Cheng, M.; Wang, W. Spatiotemporal redox heterogeneity and transient marine shelf oxygenation in the Mesoproterozoic ocean. *Geochim. Cosmochim. Acta* **2020**, *270*, 201−217.
(49) Tribovillard, N.; Algeo, T. J.; Lyons, T.; Riboulleau, A. Trace metals as paleoredox and paleoproductivity proxies: An update. *Chem. Geol.* **2006**, *232*, 12−32.
(50) Diaz, J.; Ingall, E.; Benitez-nelson, C.; Paterson, D.; De jonge, M. D.; Mcnulty, I.; Brandes, J. A. Marine polyphosphate: a key player in geologic phosphorus sequestration. *Science* **2008**, *320*, 652−655.
(51) Little, S. H.; Vance, D.; Lyons, T. W.; Mcmanus, J. Controls on trace metal authigenic enrichment in reducing sediments: insights from modern oxygen-deficient settings. *Am. J. Sci.* **2015**, *315*, 77−119.
(52) Tribovillard, N. Re-assessing copper and nickel enrichments as paleoproductivity proxies. *BSGF-Earth Sci. Bull.* **2021**, *192*, 54.
(53) Piper, D. Z.; Perkins, R. B. A modern vs. Permian black shale−−The hydrography, primary productivity, and water-column chemistry of deposition. *Chem. Geol.* **2004**, *206*, 177−197.
(54) Algeo, T. J.; Maynard, J. B. Trace-element behavior and redox facies in core shales of Upper Pennsylvanian Kansas-type cyclothems. *Chem. Geol.* **2004**, *206*, 289−318.
(55) Morse, J. W.; Luther, G. W., III Chemical influences on trace metal-sulfide interactions in anoxic sediments. *Geochim. Cosmochim. Acta* **1999**, *63*, 3373−3378.
(56) Sweere, T.; Van den boorn, S.; Dickson, A. J.; Reichart, G. J. Definition of new trace-metal proxies for the controls on organic matter enrichment in marine sediments based on Mn, Co, Mo and Cd concentrations. *Chem. Geol.* **2016**, *441*, 235−245.
(57) Brumsack, H. J. The trace metal content of recent organic carbon-rich sediments: Implications for Cretaceous black shale formation. *Palaeogeogr., Palaeoclimatol., Palaeoecol.* **2006**, *232*, 344−361.
(58) Zhai, L.; Wu, C.; Ye, Y.; Zhang, S.; Wang, Y. Fluctuations in chemical weathering on the Yangtze Block during the Ediacaran−Cambrian transition: Implications for paleoclimatic conditions and the marine carbon cycle. *Palaeogeogr., Palaeoclimatol., Palaeoecol.* **2018**, *490*, 280−292.
(59) Yeasmin, R.; Chen, D.; Fu, Y.; Wang, J.; Guo, Z.; Guo, C. Climatic-oceanic forcing on the organic accumulation across the shelf during the Early Cambrian (Age 2 through 3) in the mid-upper Yangtze Block, NE Guizhou, South China. *J. Asian Earth Sci.* **2017**, *134*, 365−386.
(60) Boström, K.; Kraemer, T.; Gartner, S. Provenance and accumulation rates of opaline silica, Al, Ti, Fe, Mn, Cu, Ni and Co in Pacific pelagic sediments. *Chem. Geol.* **1973**, *11*, 123−148.
(61) Sylvestre, G.; Evine laure, N. T.; Gus djibril, K. N.; Arlette, D. S.; Cyriel, M.; Timoléon, N.; Jean paul, N. A mixed seawater and hydrothermal origin of superior-type banded iron formation (BIF)-hosted Kouambo iron deposit, Palaeoproterozoic Nyong series, Southwestern Cameroon: constraints from petrography and geochemistry. *Ore Geol. Rev.* **2017**, *80*, 860−875.
(62) Yamamoto, K. Geochemical characteristics and depositional environments of cherts and associated rocks in the Franciscan and Shimanto Terranes. *Sediment. Geol.* **1987**, *52*, 65−108.
(63) Olivarez, A. M.; Owen, R. M. The europium anomaly of seawater: implications for fluvial versus hydrothermal REE inputs to the oceans. *Chem. Geol.* **1991**, *92*, 317−328.
(64) Elderfield, H.; Greaves, M. J. The rare-earth elements in seawater. *Nature* **1982**, *296*, 214−219.
(65) Bau, M.; Dulski, P. Distribution of yttrium and rare-earth elements in the Penge and Kuruman iron formations, Transvaal Supergroup. *South Africa. Precambrian Res.* **1996**, *79*, 37−55.
(66) Shields, G.; Stille, P. Diagenetic constraints on the use of cerium anomalies as palaeoseawater redox proxies: an isotopic and REE study of Cambrian phosphorites. *Chem. Geol.* **2001**, *175*, 29−48.
(67) Guo, Q.; Deng, Y.; Hippler, D.; Franz, G.; Zhang, J. REE and trace element patterns from organic-rich rocks of the Ediacaran−Cambrian transitional interval. *Gondwana Res.* **2016**, *36*, 94−106.
(68) Taylor, S. R.; Mclennan, S. M.; *The Continental Crust: Its Composition and Evolution*; Blackwell: Oxford, 1985.
(69) Maloof, A. C.; Porter, S. M.; Moore, J. L.; Dudás, F. O.; Bowring, S. A.; Higgins, J. A.; Fike, D. A.; Eddy, M. P. The earliest Cambrian record of animals and ocean geochemical change. *Geol. Soc. Am. Bull.* **2010**, *122*, 1731−1774.
(70) Campbell, I. H.; Squire, R. J. The mountains that triggered the Late Neoproterozoic increase in oxygen: the Second Great Oxidation Event. *Geochim. Cosmochim. Acta* **2010**, *74*, 4187−4206.
(71) Smith, M. P.; Harper, D. A. Causes of the Cambrian explosion. *Science* **2013**, *341*, 1355−1356.
(72) Korzhinsky, M. A.; Tkachenko, S. I.; Shmlovich, K. I. Discovery of a pure rhenium mineral at Kudriavy volcano. *Nature* **1994**, *369*, 51−52.
(73) Zhu, M. The origin and Cambrian explosion of animals: fossil evidences from China. *Acta Palaeontol. Sin.* **2010**, *49*, 269−287.
(74) De goeij, J. M.; Van oevelen, D.; Vermeij, M. J.; Osinga, R.; Middelburg, J. J.; De goeij, A. F.; Admiraal, W. Surviving in a marine desert: the sponge loop retains resources within coral reefs. *Science* **2013**, *342*, 108−110.
(75) Hohl, S. V.; Jiang, S. Y.; Wei, H. Z.; Pi, D. H.; Liu, Q.; Viehmann, S.; Galer, S. J. G. Cd isotopes trace periodic (bio)geochemical metal cycling at the verge of the Cambrian animal evolution. *Geochim. Cosmochim. Acta* **2019**, *263*, 195−214.
(76) Vinther, J.; Stein, M.; Longrich, N. R.; Harper, D. A. A suspension-feeding anomalocarid from the Early Cambrian. *Nature* **2014**, *507*, 496−499.
(77) Tynan, C. T. Ecological importance of the Southern Boundary of the Antarctic Circumpolar Current. *Nature* **1998**, *392*, 708−710.
(78) Cheng, M.; Li, C.; Zhou, L.; Feng, L. J.; Algeo, T. J.; Zhang, F. F.; Romaniello, S.; Jin, C. S.; Ling, H. F.; Jiang, S. Y. Transient deep-water oxygenation in the early Cambrian Nanhua Basin. *South China. Geochim. Cosmochim. Acta* **2017**, *210*, 42−58.
(79) Wei, G.; Planavsky, N. J.; Tarhan, L. G.; He, T.; Wang, D.; Shields, G. A.; Wei, W.; Ling, H. F. Highly dynamic marine redox state through the Cambrian explosion highlighted by authigenic $\delta^{238}U$ records. *Earth Planet. Sci. Lett.* **2020**, *544*, 116361.

https://doi.org/10.1021/acsomega.3c09161
ACS Omega 2024, 9, 19892−19903